Received: 14 August 2016 | Revised: 14 July 2017 | Accepted: 26 August 2017

DOI: 10.1002/fld.4463

RESEARCH ARTICLE

WILEY

Well-balanced discontinuous Galerkin method and finite volume WENO scheme based on hydrostatic reconstruction for blood flow model in arteries

Gang Li[1,2] | Olivier Delestre[3] | Li Yuan[4]

[1]School of Mathematics and Statistics, Qingdao University, Qingdao, 266071, Shandong, China

[2]Center for Computational Mechanics and Engineering Simulation, Qingdao University, Qingdao, Shandong 266071, China

[3]Université Côte d'Azur, CNRS, LJAD UMR 7351 & Polytech Nice Sophia, France

[4]LSEC and NCMIS, Institute of Computational Mathematics and Scientific/Engineering Computing, Academy of Mathematics and Systems Science, Chinese Academy of Sciences, Beijing, 100190, China

Correspondence
Gang Li, School of Mathematics and Statistics, Qingdao University, Qingdao, Shandong 266071, China.
Email: gangli1978@163.com

Funding information
Natural Science Foundation of PR China, Grant/Award Number: 11201254 and 11401332; Project for Scientific Plan of Higher Education in Shandong Province of PR China, Grant/Award Number: J12LI08, 2010CB731505; Natural Science Foundation of PR China, Grant/Award Number: 11321061 and 11261160486

Summary

The blood flow model in arteries admits the steady state solutions, for which the flux gradient is nonzero, and is exactly balanced by the source term. In this paper, by means of hydrostatic reconstruction, we construct a high order discontinuous Galerkin method, which exactly preserves the dead-man steady state, which is characterized by a discharge equal to zero (analogue to hydrostatic equilibrium). Moreover, the method maintains genuine high order of accuracy. Subsequently, we apply the key idea to finite volume weighted essentially non-oscillatory schemes and obtain a well-balanced finite volume weighted essentially non-oscillatory scheme. Extensive numerical experiments are performed to verify the well-balanced property, high order accuracy, as well as good resolution for smooth and discontinuous solutions.

KEYWORDS

blood flow model, discontinuous Galerkin method, finite volume WENO scheme, hydrostatic reconstruction, source term, well-balanced property

1 | INTRODUCTION

Numerical simulations for the blood flow model in arteries have wide applications in medical engineering,[1,2] because of the pulsatility of blood and the necessity to catch properly the waves propagation in arteries. In this paper, we are concerned with the construction of high order well-balanced discontinuous Galerkin (DG) method and finite volume weighted essentially non-oscillatory (WENO) scheme for solving the blood flow model in arteries. With some simplifying hypothesis from Navier-Stokes equations, it is possible to get the following one space dimension system for blood flow modeling[3,4]:

$$\begin{cases} A_t + Q_x = 0, \\ Q_t + \left(\alpha \frac{Q^2}{A}\right)_x + \frac{A}{\rho} p_x = -C_f \frac{Q}{A}, \end{cases} \tag{1}$$

where $A = \pi R^2$ (R being he radius of the vessel) is the cross-sectional area, $Q = Au$ denotes the discharge, u the means flow velocity, ρ stands for the blood density, p is the pressure of the artery, and α is the momentum-flux correction coefficient defined by $\alpha(x,t) = \int_S u^2 d\sigma/(Au^2)$. In the following, we consider $\alpha = 1$, which corresponds to a flat velocity profile. C_f is the viscous resistance of the flow (until Section 5.6, we consider $C_f = 0$). At steady state, we have

$$Q = constant \quad \text{and} \quad u^2/2 + p = constant, \tag{2}$$

and at steady state at rest corresponding to dead man equilibrium, we have

$$Q = u = 0 \quad \text{and} \quad p = constant, \tag{3}$$

thus we have $dp/dx = 0$. The pressure law for arteries writes

$$p - p_{ext} = K(R - R_0),$$

where R_0 is the radius of the artery at rest ($u = 0$ m/s), $A_0 = \pi R_0^2$ the cross-sectional area at rest, p_{ext} the pressure outside the tube (assumed constant), and K the arterial stiffness. Inside this coefficient K are hidden the vessel thickness, Young modulus, and Poisson ratio (see Bouchut[5] for more details). After some calculations, the 1-dimensional model can be rewritten under the following system of hyperbolic balanced laws (as shown in Xiu and Sherwin[6]):

$$\begin{cases} A_t + Q_x = 0 \\ Q_t + \left(\frac{Q^2}{A} + \frac{K}{3\rho\sqrt{\pi}} A^{3/2}\right)_x = \frac{KA}{2\rho\sqrt{\pi}\sqrt{A_0}} (A_0)_x. \end{cases} \tag{4}$$

The steady state at rest for this system, also called mechanical equilibrium, writes

$$u = 0 \quad \text{and} \quad \sqrt{A} - \sqrt{A_0} = constant. \tag{5}$$

Under the above steady state (5), the flux gradient is nonzero and is exactly balanced by the source term. Consequently, it is desirable to maintain the balancing between the flux gradient and the source term at the discrete level. In general, the standard numerical methods may not satisfy the discrete version of this balance exactly at (or near) the steady state and even introduce spurious oscillations, unless the mesh size is extremely refined. But the mesh refinement procedure is not applicable for high-dimensional problems or for big domains such as an artery network. To save the computational cost, well-balanced methods are specially introduced to preserve exactly these steady-state solutions up to machine accuracy.[7] In addition, well-balanced methods[7] can capture small perturbations on relatively coarse meshes.[8] More information about well-balanced methods can be found in the lecture note[9] and in the book.[5]

From the numerical point of view, there are many attempts based on the numerical methods for the blood flow model in the literature, eg, Sherwin et al[10] and Wang et al.[11] In recent years, there have been many interesting attempts on the well-balanced methods. For example, Delestre and Lagrée[12] presented a well-balanced finite volume scheme based on conservative governing equations.[13-15] Müller et al[16] constructed a well-balanced high order finite volume for the blood flow in elastic vessels with varying mechanical properties. Recently, Murillo et al[17] have presented an energy-balanced approximate solver for the blood flow model with upwind discretization for the source term. More recently, Wang et al[18] designed a well-balanced finite difference WENO scheme based on the modification of the source term.

The key objective of this paper is to develop a high order well-balanced DG method for the blood flow model based on the hydrostatic reconstruction, which is introduced firstly by Audusse.[19] Later, this hydrostatic reconstruction has been applied by Noelle et al[20] and Xing et al[21] for the shallow water equations as well as by Delestre and Lagrée[12] for the blood flow model. To the best of our knowledge, this is a first attempt of DG method based on hydrostatic reconstruction for the blood flow model. Subsequently, we extend the idea in the present DG method to finite volume WENO scheme and obtain a well-balanced finite volume WENO scheme.

Moreover, we also mention some attempts for deriving well-balanced methods for other model equations, such as previous studies[22-26] for shallow water equations over non-flat bottom topography and previous works[27-31] for Euler equations under gravitational fields.

This paper is organized as follows: We briefly review the key ideas of the DG methods and the finite volume WENO schemes in Section 2. In Section 3, we propose a high order well-balanced DG method for the blood flow model. We generalize the idea for the DG method to the finite volume WENO scheme in Section 4. Extensive numerical experiments are performed in Section 5. Some conclusions are given in Section 6.

2 | A REVIEW OF HIGH ORDER DG METHOD AND FINITE VOLUME WENO SCHEME

In this section, we briefly review the basic ideas of DG methods and finite volume WENO schemes. For more details about these subjects, we refer to previous studies.[32-36]

To begin with, we apply a 1-dimensional scalar hyperbolic conservation law to present the DG method

$$w_t + f(w)_x = 0. \tag{6}$$

Firstly, we divide the interval $I = [a, b]$ into N subintervals and denote the cells by $I_j = [x_{j-\frac{1}{2}},\ x_{j+\frac{1}{2}}]$ for $j = 1, \cdots, N$. The center of each cell is $x_j = \frac{1}{2}\left(x_{j-\frac{1}{2}} + x_{j+\frac{1}{2}}\right)$, and the mesh size is denoted by $h_j = x_{j+\frac{1}{2}} - x_{j-\frac{1}{2}}$, with $h = \max\limits_{1\le j\le N} h_j$ being the maximal mesh size.

Under the framework of the DG methods,[32,33] we seek an approximation w_h to w, which belongs to a finite dimensional space

$$V_h^k = \left\{v : v|_{I_j} \in P^k(I_j),\ j = 1, 2, \cdots, N\right\}. \tag{7}$$

Note that functions in V_h^k are allowed to have discontinuities across element interfaces. The standard DG method for (6) is given by

$$\int_{I_j} \partial_t w_h v_h \mathrm{d}x + \hat{F}_{j+\frac{1}{2}} v_h\left(x^-_{j+\frac{1}{2}}\right) - \hat{F}_{j-\frac{1}{2}} v_h\left(x^+_{j-\frac{1}{2}}\right) - \int_{I_j} f(w_h)\partial_x v_h \mathrm{d}x = 0, \quad \text{for} \quad \forall\, v_h \in V_h^k, \tag{8}$$

with $\hat{F}_{j+\frac{1}{2}} = F\left(w^-_{h,j+\frac{1}{2}},\ w^+_{h,j+\frac{1}{2}}\right)$ being the numerical flux. We denote by $w^+_{h,j+\frac{1}{2}}$ and $w^-_{h,j+\frac{1}{2}}$ the limit values of w_h at $x_{j+\frac{1}{2}}$ from the right cell I_{j+1} and from the left cell I_j, respectively. The simplest and less expensive flux is the Lax-Friedrichs flux:

$$F(a, b) = \frac{1}{2}(f(a) + f(b) - \alpha(b - a)), \tag{9}$$

where $\alpha = \max\limits_{w} \left|f'(w)\right|$.

Under the framework of the finite volume WENO schemes for (6), we seek the numerical solution $\bar{w}_j(t)$, which approximate the cell averages $\bar{w}(x_j, t) = \frac{1}{\Delta x}\int_{I_j} w(x, t)\ \mathrm{d}\ x$. The conservative finite volume WENO scheme has the following form:

$$\frac{\mathrm{d}}{\mathrm{d}t}\bar{w}_j(t) + \frac{1}{\Delta x}\left(\hat{F}_{j+\frac{1}{2}} - \hat{F}_{j-\frac{1}{2}}\right) = 0, \tag{10}$$

with $\hat{F}_{j+\frac{1}{2}} = F\left(w^-_{j+\frac{1}{2}}, w^+_{j+\frac{1}{2}}\right)$ being the numerical flux. Herein, $w^-_{j+\frac{1}{2}}$ and $w^+_{j+\frac{1}{2}}$ are the high order pointwise approximations to $w\left(x_{j+\frac{1}{2}}, t\right)$ from left and right, respectively. They are computed through the neighboring cell average values by a high order WENO reconstruction procedure. Basically, for a $(2k-1)$-th order WENO scheme, we first compute k reconstructed boundary values $w^{(k),\pm}_{j+\frac{1}{2}}$ corresponding to different candidate stencils. Then by providing each value a nonlinear weight that indicates the smoothness of the corresponding stencil, we define the $(2k-1)$-th order WENO reconstruction $w^{\pm}_{j+\frac{1}{2}}$ as a convex combination of all these k reconstructed values. Eventually, the WENO reconstruction can be written out as:

$$w^+_{j+\frac{1}{2}} = \sum_{r=-k+1}^{k} \omega_r \bar{w}_{j+r}, \qquad w^-_{j+\frac{1}{2}} = \sum_{r=-k}^{k-1} \tilde{\omega}_r \bar{w}_{j+r}, \tag{11}$$

the coefficients ω_r and $\tilde{\omega}_r$ depend nonlinearly on the smoothness indicators involving the cell averages $\bar{w}$. For hyperbolic systems of conservation laws, we usually apply the local characteristic decomposition procedure with more computational

cost to obtain good numerical results, which is more robust than a component by component version. The complete algorithm can be found in Shu.[34,35]

3 | WELL-BALANCED DG METHOD FOR THE BLOOD FLOW MODEL

In this section, we present a well-balanced DG method for the blood flow model (4). For the steady state (5), the first equation $Q_x = 0$ is satisfied exactly for any consistent method since Q due to $u = 0$. Then, we focus on the second equation, which can be denoted by

$$Q_t + f(U)_x = S(A, A_0), \tag{12}$$

where $U = (A, Q)^T$ with the superscript T denoting the transpose.

In the DG method, U is approximated by a piecewise polynomial $U_h \in V_h^k$. Moreover, we also project A_0 into the same space V_h^k to obtain an approximation $(A_0)_h$ for A_0. This implies that $\sqrt{A_h} - \sqrt{(A_0)_h} = constatn$ if $\sqrt{A} - \sqrt{A_0} = constant$.

Our DG method has the following form:

$$\int_{I_j} \partial_t Q_h v_h \mathrm{d}x + \hat{F}^l_{j+\frac{1}{2}} v_h\left(x^-_{j+\frac{1}{2}}\right) - \hat{F}^r_{j-\frac{1}{2}} v_h\left(x^+_{j-\frac{1}{2}}\right) - \int_{I_j} f(U_h)\partial_x v_h \mathrm{d}x = \int_{I_j} S\left(A_h, (A_0)_h\right) v_h \mathrm{d}x. \tag{13}$$

The numerical fluxes $\hat{F}^l_{j+\frac{1}{2}}$ and $\hat{F}^r_{j-\frac{1}{2}}$ will be presented in Section 3.1.

Compared with the standard DG method (8), we can observe that the single valued numerical fluxes $\hat{F}_{j+\frac{1}{2}}$ and $\hat{F}_{j-\frac{1}{2}}$ have been replaced by the left flux $\hat{F}^l_{j+\frac{1}{2}}$ and the right flux $\hat{F}^r_{j-\frac{1}{2}}$ in (13), respectively. In fact, we can rewrite the present DG method (13) as follows:

$$\begin{aligned} &\int_{I_j} \partial_t Q_h v_h \mathrm{d}x + \hat{F}_{j+\frac{1}{2}} v_h\left(x^-_{j+\frac{1}{2}}\right) - \hat{F}_{j-\frac{1}{2}} v_h\left(x^+_{j-\frac{1}{2}}\right) - \int_{I_j} f(U_h)\partial_x v_h \mathrm{d}x \\ &= \int_{I_j} S\left(A_h, (A_0)_h\right) v_h \mathrm{d}x + \left(\hat{F}_{j+\frac{1}{2}} - \hat{F}^l_{j+\frac{1}{2}}\right) v_h\left(x^-_{j+\frac{1}{2}}\right) - \left(\hat{F}_{j-\frac{1}{2}} - \hat{F}^r_{j-\frac{1}{2}}\right) v_h\left(x^+_{j-\frac{1}{2}}\right), \end{aligned} \tag{14}$$

where $\hat{F}_{j+\frac{1}{2}} = F\left(U^-_{h,j+\frac{1}{2}}, U^+_{h,j+\frac{1}{2}}\right)$. The left hand side of (14) is the traditional DG method, and the right hand side is our approximation to the source term. Herein, we point out that $\hat{F}_{j+\frac{1}{2}} - \hat{F}^l_{j+\frac{1}{2}}$ and $\hat{F}_{j-\frac{1}{2}} - \hat{F}^r_{j-\frac{1}{2}}$ are high order correction terms at the level of $O(\Delta x)^{k+1}$. Therefore, the present DG method (14) is a $(k+1)$-th order conservative method and will converge to the weak solution accordingly.

3.1 | The numerical fluxes based on hydrostatic reconstruction

Herein, we take the numerical fluxes $\hat{F}^l_{j+\frac{1}{2}}$ and $\hat{F}^r_{j-\frac{1}{2}}$ in (13) with the following forms:

$$\hat{F}^l_{j+\frac{1}{2}} = f\left(U^{*,-}_{h,j+\frac{1}{2}}\ U^{*,+}_{h,j+\frac{1}{2}}\right) + \begin{pmatrix} 0 \\ \frac{K}{3\rho\sqrt{\pi}}\left(A^-_{h,j+\frac{1}{2}}\right)^{\frac{3}{2}} - \frac{K}{3\rho\sqrt{\pi}}\left(A^{*,-}_{h,j+\frac{1}{2}}\right)^{\frac{3}{2}} \end{pmatrix} \tag{15}$$

and

$$\hat{F}^r_{j-\frac{1}{2}} = f\left(U^{*,-}_{h,j-\frac{1}{2}}\ U^{*,+}_{h,j-\frac{1}{2}}\right) + \begin{pmatrix} 0 \\ \frac{K}{3\rho\sqrt{\pi}}\left(A^+_{h,j-\frac{1}{2}}\right)^{\frac{3}{2}} - \frac{K}{3\rho\sqrt{\pi}}\left(A^{*,+}_{h,j-\frac{1}{2}}\right)^{\frac{3}{2}} \end{pmatrix}. \tag{16}$$

Herein, the construction of the numerical fluxes $\hat{F}^r_{j-\frac{1}{2}}$ and $\hat{F}^l_{j+}$ is vital to the preservation of the well-balanced property. As a matter of fact, our key idea is to make sure that

$$\hat{F}^l_{j+\frac{1}{2}} = f\left(U^-_{h,j+\frac{1}{2}}\right), \quad \text{and} \quad \hat{F}^r_{j-\frac{1}{2}} = f\left(U^+_{h,j-\frac{1}{2}}\right).$$

Accordingly, we take the reconstruction values $\sqrt{A^{*,+}_{h,j+\frac{1}{2}}}$ and $\sqrt{A^{*,-}_{h,j+\frac{1}{2}}}$ in (15) and (16) as follows:

$$\begin{aligned}
\sqrt{A^{*,+}_{h,j+\frac{1}{2}}} &= \max\left\{0,\ \sqrt{\overset{+}{\mathrm{A}}_{h,j+\frac{1}{2}}} - \sqrt{(A_0)^{+}_{h,j+\frac{1}{2}}} + \max\left\{\sqrt{(A_0)^{-}_{h,j+\frac{1}{2}}},\ \sqrt{(A_0)^{+}_{h,j+\frac{1}{2}}}\right\}\right\},\\
\sqrt{A^{*,-}_{h,j+\frac{1}{2}}} &= \max\left\{0,\ \sqrt{\overset{-}{\mathrm{A}}_{h,j+\frac{1}{2}}} - \sqrt{(A_0)^{-}_{h,j+\frac{1}{2}}} + \max\left\{\sqrt{(A_0)^{-}_{h,j+\frac{1}{2}}},\ \sqrt{(A_0)^{+}_{h,j+\frac{1}{2}}}\right\}\right\},
\end{aligned} \tag{17}$$

which is the hydrostatic reconstruction adapted to blood flow model. This approach of the hydrostatic reconstruction has been first developed for shallow water equation by Audusse et al[19] and has been later applied in Noelle et al[20] and Xing and Shu[21] for shallow water equations. Moreover, this approach has also been adopted by Delestre and Lagrée[12] for the blood flow model.

Then, based on (17), we can obtain $A^{*,\pm}_{h,j+\frac{1}{2}}$ and subsequently get

$$U^{*,\pm}_{h,j+\frac{1}{2}} = \begin{pmatrix} A^{*,\pm}_{h,j+\frac{1}{2}} \\ Q^{\pm}_{h,j+\frac{1}{2}} \end{pmatrix}. \tag{18}$$

In a similar way, we can obtain

$$U^{*,\pm}_{h,j-\frac{1}{2}} = \begin{pmatrix} A^{*,\pm}_{h,j-\frac{1}{2}} \\ Q^{\pm}_{h,j-\frac{1}{2}} \end{pmatrix}. \tag{19}$$

We assume that U_h being the numerical approximation to U is a steady-state solution of the equation $Q_t + f(U_h)_x = S(A_h, (A_0)_h)$. This fact is true since $\sqrt{A_h} - \sqrt{(A_0)_h} = constant$ and $u_h = 0$, which subsequently imply $\left(\frac{K}{3\rho\sqrt{\pi}}A_h^{\frac{3}{2}}\right)_x = S(A_h, (A_0)_h)$, or

$$\partial_x f(U_h) = S(A_h, (A_0)_h). \tag{20}$$

3.2 | Well-balanced method

All these together lead to a well-balanced DG method for the blood flow model, as outlined in the following proposition.

Proposition 1. *For the blood flow model (4), the semi-discrete DG method (13), combined with (15) and (16) as well as (17), is well-balanced for the steady state solutions (5).*

Proof. For the steady state solutions (5), the first equation $\partial_x Q = 0$ is satisfied exactly for any consistent method since $Q = Au = 0$ due to $u = 0$.

At the steady state, we have $\sqrt{A_h} - \sqrt{(A_0)_h} = constant$ and $u_h = 0$. From (17), we can easily observe $A^{*,-}_{h,j+\frac{1}{2}} = A^{*,+}_{h,j+\frac{1}{2}}$. Subsequently, we can obtain

$$\hat{F}^{l}_{j+\frac{1}{2}} = \begin{pmatrix} 0 \\ \frac{K}{3\rho\sqrt{\pi}}\left(A^{*,-}_{h,j+\frac{1}{2}}\right)^{\frac{3}{2}} \end{pmatrix} + \begin{pmatrix} 0 \\ \frac{K}{3\rho\sqrt{\pi}}\left(A^{-}_{h,j+\frac{1}{2}}\right)^{\frac{3}{2}} - \frac{K}{3\rho\sqrt{\pi}}\left(A^{*,-}_{h,j+\frac{1}{2}}\right)^{\frac{3}{2}} \end{pmatrix} = f\left(U^{-}_{h,j+\frac{1}{2}}\right), \tag{21}$$

due to (15). Similarly, we have

$$\hat{F}^{r}_{j-\frac{1}{2}} = f\left(U^{+}_{h,j-\frac{1}{2}}\right). \tag{22}$$

Then, the residue R in (13) for steady-state solutions reduces to

$$\begin{aligned} R &= \hat{F}^l_{j+\frac{1}{2}} v_h\left(x^-_{j+\frac{1}{2}}\right) - \hat{F}^r_{j-\frac{1}{2}} v_h\left(x^+_{j-\frac{1}{2}}\right) - \int_{I_j} f(U_h)\partial_x v_h \mathrm{d}x - \int_{I_j} S(A_h,(A_0)_h)v_h \mathrm{d}x \\ &= f\left(U^-_{hj+\frac{1}{2}}\right) v_h\left(x^-_{j+\frac{1}{2}}\right) - f\left(U^+_{hj-\frac{1}{2}}\right) v_h\left(x^+_{j-\frac{1}{2}}\right) - \int_{I_j} f(U_h)\partial_x v_h \mathrm{d}x - \int_{I_j} S(A_h,(A0)_h)v_h \mathrm{d}x \\ &= \int_{I_j} \partial_x f(U_h) v_h \mathrm{d}x - \int_{I_j} S(A_h,(A0)_h)v_h \mathrm{d}x \\ &= \int_{I_j} \left(\partial_x f(U_h) - S(A_h,(A0)_h)\right) v_h \mathrm{d}x \\ &= 0, \end{aligned} \tag{23}$$

where the second equality is due to (21) and (22), the third equality follows from a simple integration by parts, and the last equality derives from the equality (20). □

For the temporal discretization, high order total variation diminishing (TVD) Runge-Kutta method[37] can be used. In the numerical section of this paper, we apply the third-order Runge-Kutta method:

$$\begin{aligned} lclU^{(1)} &= U^n + \Delta t \mathcal{F}(U^n) \\ U^{(2)} &= \frac{3}{4}U^n + \frac{1}{4}\left(U^{(1)} + \Delta t \mathcal{F}(U^{(1)})\right) \\ U^{n+1} &= \frac{1}{3}U^n + \frac{2}{3}\left(U^{(2)} + \Delta t \mathcal{F}(U^{(2)})\right), \end{aligned} \tag{24}$$

with $\mathcal{F}(U)$ being the spatial operator.

4 | WELL-BALANCED FINITE VOLUME WENO SCHEME FOR THE BLOOD FLOW MODEL

In this section, we generalize the idea of the well-balanced DG method in Section 3 to design a well-balanced finite volume WENO scheme for the blood flow model. The basic idea is the same as that for the DG method. The only extra step is due to the fact that we only have the reconstructed pointwise values $U^{\pm}_{j+\frac{1}{2}}$ and would need to first define an approximation function U_h. We can then follow the procedure as before.

For sake of the well-balanced property, we only need to consider the second equation of the model (4), ie, (12). Our well-balanced finite volume WENO scheme is given by

$$\frac{\mathrm{d}}{\mathrm{d}t}\bar{Q}_j(t) + \frac{1}{\Delta x}\left(\hat{F}^l_{j+\frac{1}{2}} - \hat{F}^r_{j-\frac{1}{2}}\right) = \frac{1}{\Delta x}\int_{I_j} S(A,A_0)\mathrm{d}x, \tag{25}$$

with $\hat{F}^l_{j+\frac{1}{2}}$ and $\hat{F}^r_{j-\frac{1}{2}}$ being the left and right numerical fluxes as defined in Section 3.

Remark 1. To construct a high order polynomial A_h on the cell I_j, we apply interpolation based on the boundary values $A^+_{j-\frac{3}{2}}, A^+_{j-\frac{1}{2}}, A^-_{j+\frac{1}{2}}$, and $A^-_{j+\frac{3}{2}}$, which come from the cell averages $\bar{A}_j$ by means of WENO reconstruction procedure. In a similar way, we use the same interpolation on A_0 to obtain a polynomial $(A_0)_h$.

Similarly, we get the following proposition for the well-balanced finite volume WENO scheme as for the DG method.

Proposition 2. *For the blood flow model (4), the semi-discrete finite volume WENO scheme (25), combined with (15) and (16) as well as (17), are well-balanced for the steady state solutions (5).*

Proof. In fact, for the second equation, the residue R in (25) reduces to

$$\begin{aligned} R &= \hat{F}^l_{j+\frac{1}{2}} - \hat{F}^r_{j-\frac{1}{2}} - \int_{I_j} S(A_h, (A_0)_h)\mathrm{d}x \\ &= f\left(U^-_{h,j+\frac{1}{2}}\right) - f\left(U^+_{h,j-\frac{1}{2}}\right) - \int_{I_j} S(A_h, (A_0)_h)\mathrm{d}x \\ &= \int_{I_j} \partial_x f(U_h)\mathrm{d}x - \int_{I_j} S(A_h, (A_0)_h)\mathrm{d}x \\ &= \int_{I_j} \left(\partial_x f(U_h) - S(A_h, (A0)_h)\right)\mathrm{d}x \\ &= 0, \end{aligned} \tag{26}$$

where the second equality is due to (15) and (16), the third equality follows from a simple integration by parts, and the last equality follows from (20). Then, this completes the proof correspondingly. □

For the temporal discretization, we also apply the third-order Runge-Kutta method (24) as it is also applied in Xing and Shu.[21,38]

5 | NUMERICAL RESULTS

In this section, we perform extensive numerical experiments to demonstrate the performance of the proposed third-order well-balanced DG method and the fifth-order well-balanced finite volume WENO scheme. In all the computations, we apply the third-order TVD Runge-Kutta method (24) for the time discretization. For the third-order DG method, the CFL number is 0.18. For fifth-order finite volume WENO schemes, the CFL number is taken as 0.6.

5.1 | To test the order of accuracy

We apply the following example to test the order of accuracy of the resulting method. The initial conditions are defined by

$$A(x,0) = \sin^2(\pi x), \quad Q(x,0) = \sin(\pi x) + \cos(\pi x), \quad \text{and} \qquad A_0(x) = \cos^2(\pi x),$$

on a computational domain $[0, 2]$ based on the following parameters: $K = 1 \times 10^8$ Pa/m, $\rho = 1060$ kg/m^3.

We impose this problem with periodic boundary conditions at the 2 endpoints. Then, we solve this example up to $t = 0.01$ seconds and get reference solutions on a mesh with 2000 cells. We present the errors and the order of accuracy in Table 1. It is clear that the DG method and the WENO scheme all obtain their expected order of accuracy.

5.2 | The ideal tourniquet

This example is similar with the dam break problem in shallow water equations, namely, Stoker's solution.[39] Here, we consider the analogue of this problem in blood flow model: A tourniquet is applied, and we remove it instantaneously.

TABLE 1 L^1 errors and numerical orders of accuracy for the example of Section 5.1

	DG Method				WENO Scheme			
	A		Q		A		Q	
N	L^1error	Order	L^1error	Order	L^1error	Order	L^1error	Order
50	2.32E-3		2.59E-02		3.34E-3		3.34E-2	
100	8.03E-4	1.53	8.48E-03	1.61	5.00E-4	2.74	5.25E-3	2.67
200	2.14E-4	1.91	2.23E-03	1.93	5.83E-5	3.10	5.55E-4	3.24
400	3.96E-5	2.43	4.19E-04	2.41	4.68E-6	3.64	3.70E-5	3.91
800	5.49E-6	2.85	5.81E-05	2.85	2.25E-7	4.38	1.60E-6	4.53
1600	6.36E-7	3.11	7.11E-06	3.03	6.92E-9	5.03	4.90E-8	5.03

Abbreviations: DG, discontinuous Galerkin; WENO, weighted essentially non-oscillatory.

We consider the following initial conditions

$$A(x,0) = \begin{cases} \pi R_L^2 & \text{if } x \le 0, \\ \pi R_R^2 & \text{otherwise,} \end{cases} \quad \text{and} \quad Q(x,0) = 0,$$

on a computational domain $[-0.04, 0.04]$ based on the following parameters: $K = 1 \times 10^7$ Pa/m, $\rho = 1060$ kg/m^3, $R_L = 5 \times 10^{-3}$ m, $R_R = 4 \times 10^{-3}$ m.

We impose this problem with transmissive boundary conditions. Then, we solve this example on a mesh with 200 cells up to $t = 0.005$ seconds and present the numerical solutions against the exact ones in Figures 1 and 2. In addition, we also run the same numerical test using the non–well-balanced DG method and the non–well-balanced WENO scheme, with a straightforward numerical treatment of the source term, and show their results in Figures 1 and 2, respectively, for comparison. It is obvious that the results of the well-balanced DG method and the well-balanced WENO scheme are in good agreement with the exact solutions and keep steep shock transitions, while the results of the non–well-balanced ones fail to fit well with the exact solutions.

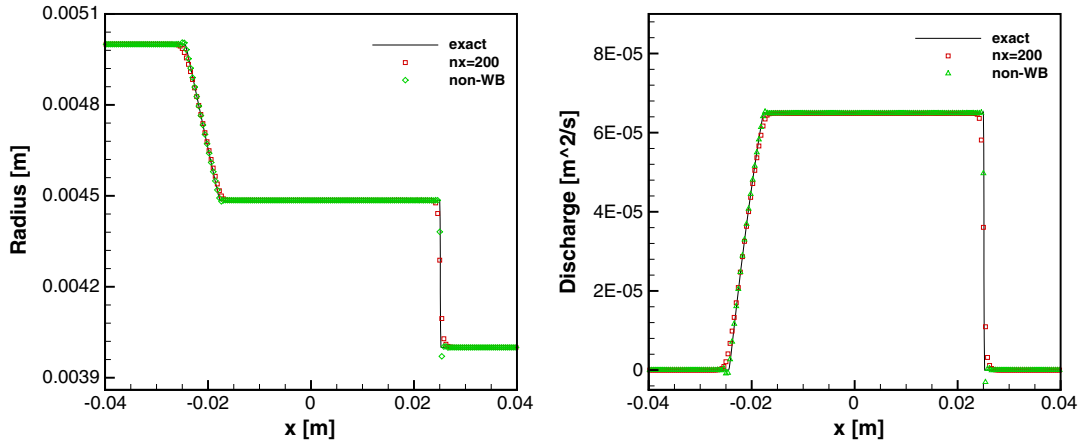

FIGURE 1 DG method: The numerical solutions of the ideal tourniquet problem in Section 5.2 on a mesh with 200 cells at $t = 0.005$ seconds and those of the non–well-balanced (denoted by non-WB) method. Radius (left) and discharge (right) [Colour figure can be viewed at wileyonlinelibrary.com]

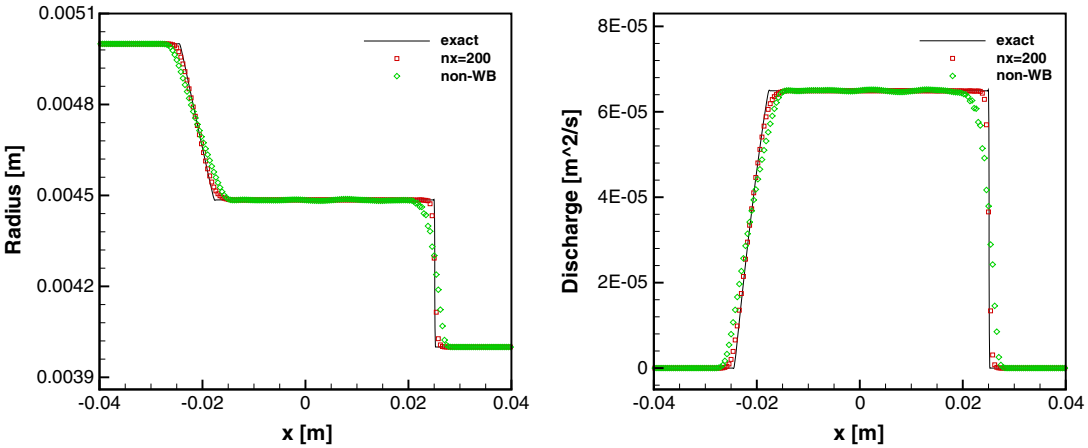

FIGURE 2 WENO scheme: The numerical solutions of the ideal tourniquet problem in Section 5.2 on a mesh with 200 cells at $t = 0.005$ seconds and those of the non–well-balanced (denoted by non-WB) scheme. Radius (left) and discharge (right) [Colour figure can be viewed at wileyonlinelibrary.com]

5.3 | Wave equation

The following quasi-stationary test case has been proposed by Delestre and Lagrée[12] and is chosen to demonstrate the capability of the proposed method to compute the spreading of a small perturbation of a steady state. In that case, we recover the behavior of the wave equation.

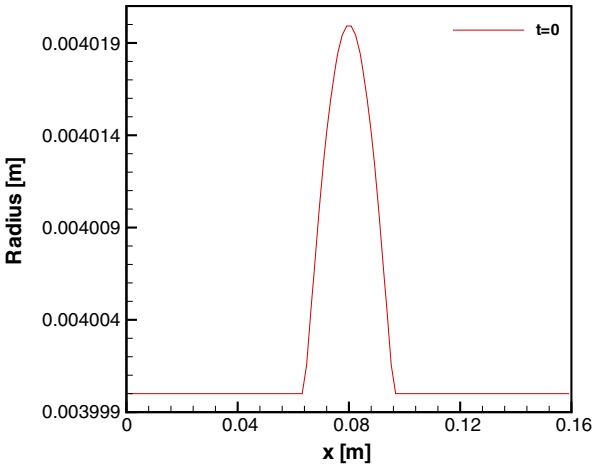

FIGURE 3 The initial radius of the wave equation problem in Section 5.3 [Colour figure can be viewed at wileyonlinelibrary.com]

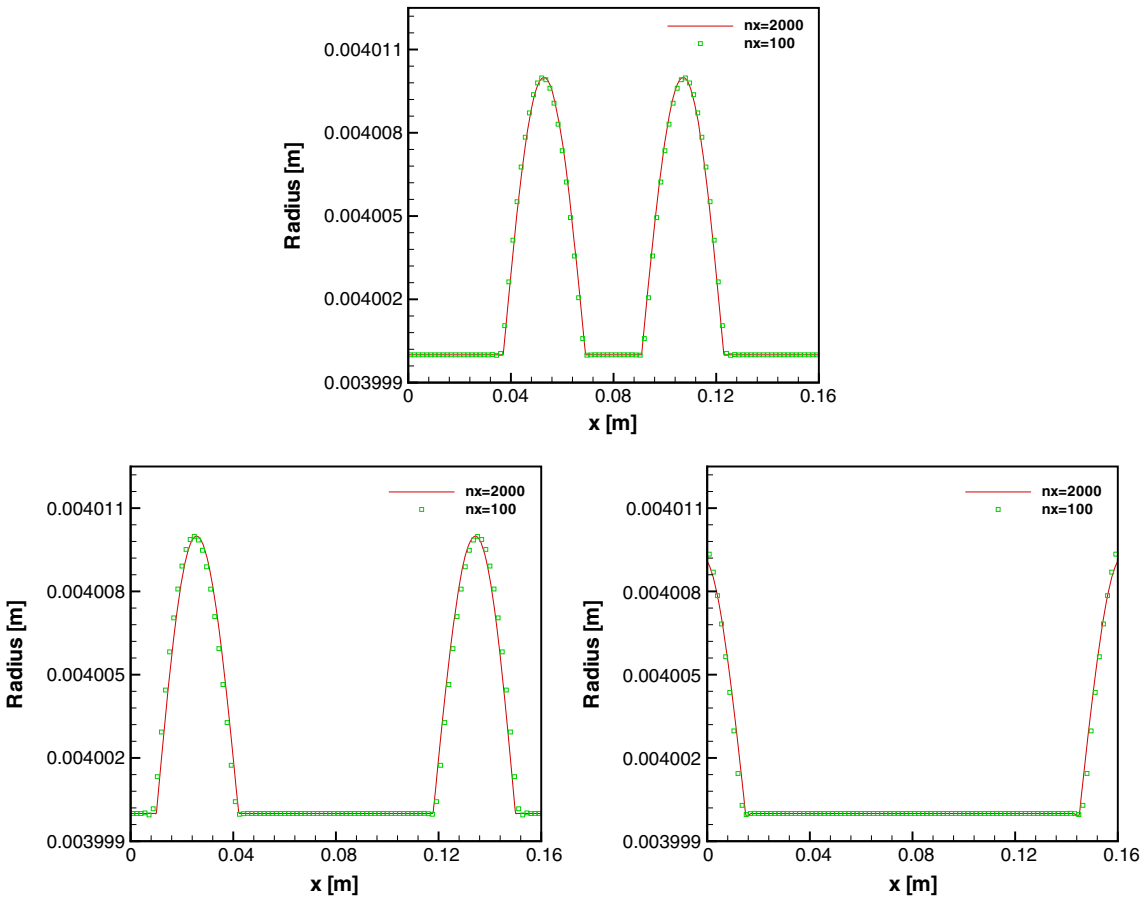

FIGURE 4 DG method: The numerical solutions of the wave equation problem in Section 5.3 on a mesh with 100 cells. Radius at $t = 0.002$ seconds (upper), $t = 0.004$ seconds (lower left), and $t = 0.006$ seconds (lower right), respectively [Colour figure can be viewed at wileyonlinelibrary.com]

Herein, we apply the following initial data:

$$A(x,0) = \begin{cases} \pi R_0^2 & \text{if } x \in \left[0, \frac{40L}{100}\right] \cup \left[\frac{60L}{100}, L\right], \\ \pi R_0^2 \left[1 + \epsilon \sin\left(\pi \frac{x - 40L/100}{20L/100}\right)\right]^2 & \text{if } x \in \left[\frac{40L}{100}, \frac{60L}{100}\right], \end{cases} \qquad Q(x,0) = 0,$$

on a computational domain $[0, 0.16]$ coupled with transmissive boundary conditions. The following parameters have been used for this example: $\epsilon = 5 \times 10^{-3}$, $K = 10^8$ Pa/m, $\rho = 1060$ kg/m^3, $R_0 = 4 \times 10^{-3}$ m, and $L = 0.16$ m.

The initial radius is presented in Figure 3. We show the numerical solutions on a mesh with 100 cells at $t = 0.002$, 0.004, and 0.006 seconds, respectively, against the exact solutions in Figures 4 and 5. The figures strongly suggest that the numerical solutions of the well-balanced DG method and the well-balanced WENO scheme agree well with the reference ones.

5.4 | The man at eternal rest

The purpose of this example is to verify that the current DG method and the WENO scheme indeed maintain the well-balanced property.

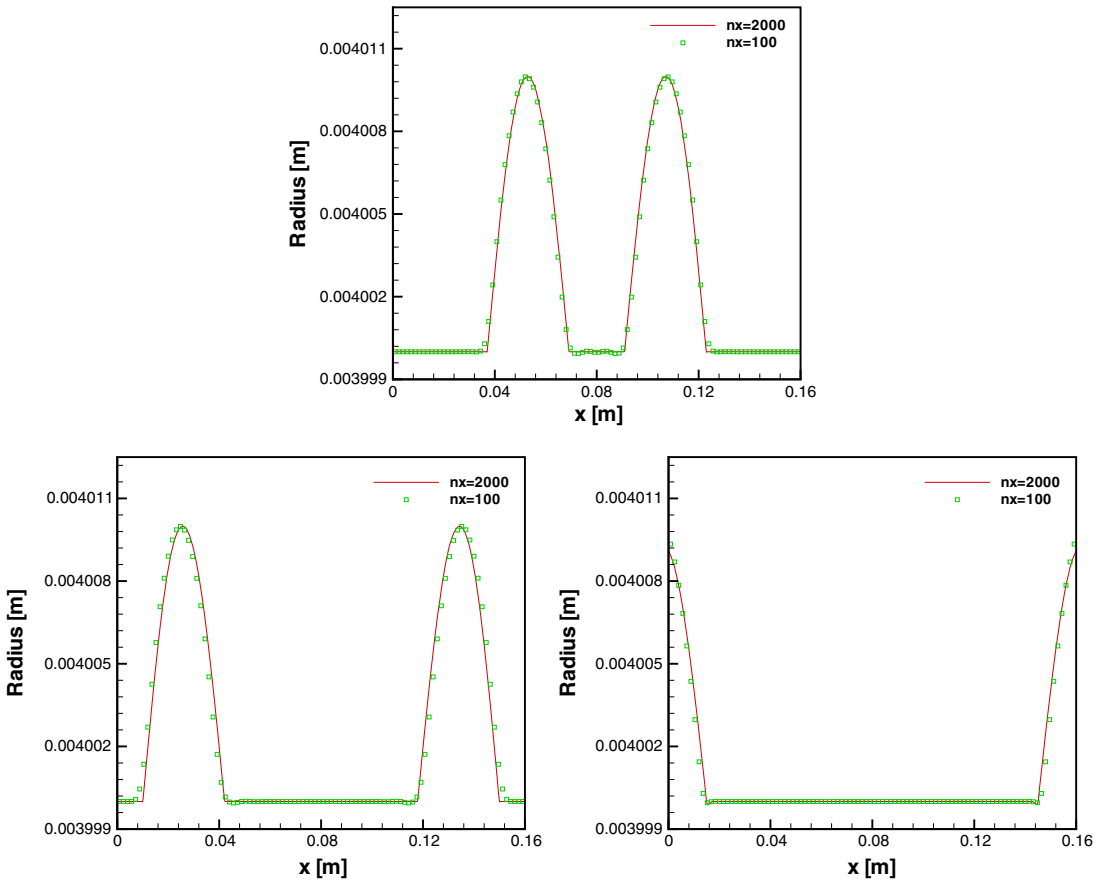

FIGURE 5 WENO scheme: The numerical solutions of the wave equation problem in Section 5.3 on a mesh with 100 cells. Radius at $t = 0.002$ seconds (upper), $t = 0.004$ seconds (lower left), and $t = 0.006$ seconds (lower right), respectively [Colour figure can be viewed at wileyonlinelibrary.com]

Herein, we consider a configuration with no flow and with a change of radius $R_0(x)$, this is the case for a dead man with an aneurism. Thus, for the initial conditions, the section of the artery is not constant with the following form

$$R(x,0) = R_0(x) = \begin{cases} \tilde{R} & \text{if } x \in [0, x_1] \cup [x_4, L], \\ \tilde{R} + \frac{\Delta R}{2}\left[\sin\left(\frac{x-x_1}{x_2-x_1}\pi - \frac{\pi}{2}\right) + 1\right] & \text{if } x \in [x_1, x_2], \\ \tilde{R} + \Delta R & \text{if } x \in [x_2, x_3], \\ \tilde{R} + \frac{\Delta R}{2}\left[\cos\left(\frac{x-x_3}{x_4-x_3}\pi\right) + 1\right] & \text{if } x \in [x_3, x_4], \end{cases}$$

on a computational domain $[0, 0.14]$ with $\tilde{R} = 4 \times 10^{-3}$ m, $\Delta R = 10^{-3}$ m, $K = 10^8$ Pa/m, $\rho = 1060$ kg/m^3, $L = 0.14$ m, $x_1 = 10^{-2}$ m, $x_2 = 3.05 \times 10^{-2}$ m, $x_3 = 4.95 \times 10^{-2}$ m, and $x_4 = 7 \times 10^{-2}$ m. In addition, the initial velocity is zero. We impose this problem with transmissive boundary conditions and compute this example up to $t = 5$ seconds.

To show that the well-balanced property is maintained up to the machine round off error, tests are run using single, double, and quadruple precisions, respectively, on a mesh with 100. We present the L^1 and L^∞ errors for A and Q in Table 2. It can be clearly seen that the L^1 and L^∞ errors are all at the level of round off errors associated with different precisions, which verify that the current DG method and the WENO scheme indeed maintain the steady state and thus their well-balanced property accordingly.

Moreover, we also ran the same test case using the non–well-balanced DG method and the non–well-balanced WENO scheme, with a straightforward integration of the source term, and show their results in Figures 6 and 7 for the sake of comparison. It is obvious that the results of the DG method and the WENO scheme are in good agreement with the reference solutions for the case, while the non–well-balanced ones produce spurious oscillations.

TABLE 2 L^1 and L^∞ error for different precisions for the man at eternal rest in Section 5.4

	DG Method				WENO Scheme			
	L^1error		L^∞ error		L^1error		L^∞ error	
Precision	A	Q	A	Q	A	Q	A	Q
Single	1.04E-07	1.46E-07	3.96E-07	6.38E-07	2.41E-07	5.47E-07	3.25E-07	1.25E-07
Double	2.82E-16	2.82E-16	5.38E-16	4.42E-15	3.79E-16	3.89E-16	5.91E-16	6.56E-16
Quadruple	2.59E-31	5.69E-32	2.52E-33	1.58E-32	5.93E-32	4.63E-31	8.04E-33	2.39E-32

Abbreviations: DG, discontinuous Galerkin; WENO, weighted essentially non-oscillatory.

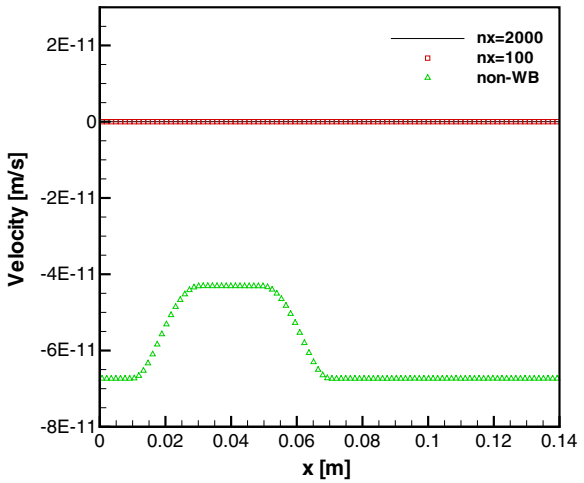

FIGURE 6 DG method: The man at eternal rest problem in Section 5.4 at $t = 5$ seconds. The results of the well-balanced method with 100 and 2000 cells and those of the non–well-balanced (denoted by non-WB) method with 100 cells [Colour figure can be viewed at wileyonlinelibrary.com]

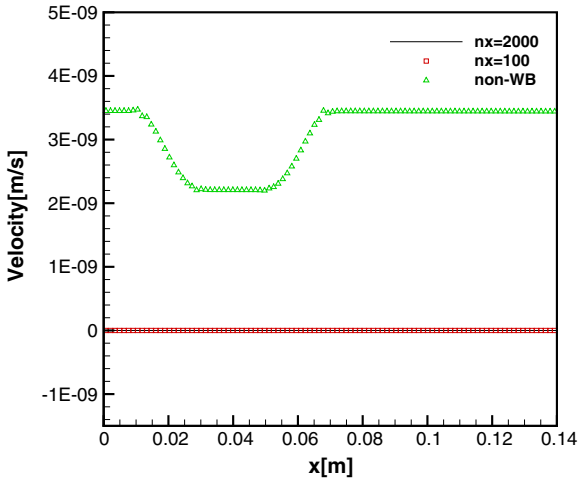

FIGURE 7 WENO scheme: The man at eternal rest problem in Section 5.4 at $t = 5$ seconds. The results of the well-balanced scheme with 200 and 2000 cells and those of the non–well-balanced (denoted by non-WB) scheme with 100 cells [Colour figure can be viewed at wileyonlinelibrary.com]

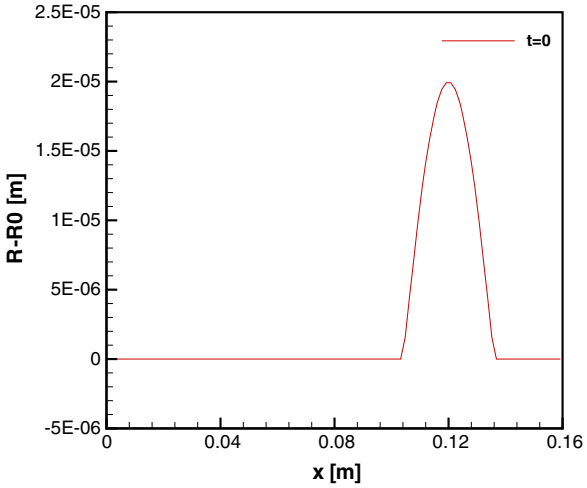

FIGURE 8 The initial error $R - R_0$ of the propagation of a pulse to an expansion in Section 5.5 [Colour figure can be viewed at wileyonlinelibrary.com]

5.5 | Propagation of a pulse to an expansion

Firstly, we test the case of a pulse in a section R_R passing trough an expansion: $A_L > A_R$, taking the following parameters: $K = 1.0 \times 10^8$ Pa/m, $L = 0.16$ m, $\rho = 1060$ kg/m^3, $R_L = 5 \times 10^{-3}$ m, $R_R = 4 \times 10^{-3}$ m, $\Delta R = 1.0 \times 10^{-3}$ m. We take a decreasing shape on a rather small scale:

$$R_0(x) = \begin{cases} R_R + \Delta R & \text{if } x \in [0, x_1], \\ R_R + \frac{\Delta R}{2}\left[1 + \cos\left(\frac{x - x_1}{x_2 - x_1}\pi\right)\right] & \text{if } x \in [x_1, x_2], \\ R_R & \text{else,} \end{cases}$$

with $x_1 = \frac{19L}{40}$, $x_2 = \frac{L}{2}$. As initial conditions, we consider a fluid at rest ($Q(x, 0) = 0$ m^3/s) and the following perturbation of radius:

$$R(x, 0) = \begin{cases} R_0(x)\left[1 + \epsilon \sin\left(\frac{100}{20L}\pi\left(x - \frac{65L}{100}\right)\right)\right] & \text{if } x \in \left[\frac{65L}{100}, \frac{85L}{100}\right], \\ R_0(x) & \text{else,} \end{cases}$$

with $\epsilon = 5.0 \times 10^{-3}$ and transmissive boundary conditions.

We present the initial error $R - R_0$ at time $t = 0$ seconds in Figure 8 and present the numerical results against the reference solutions at $t = 0.002$ seconds and $t = 0.006$ seconds in Figures 9 and 10. We get 2 travelling waves, one spreading

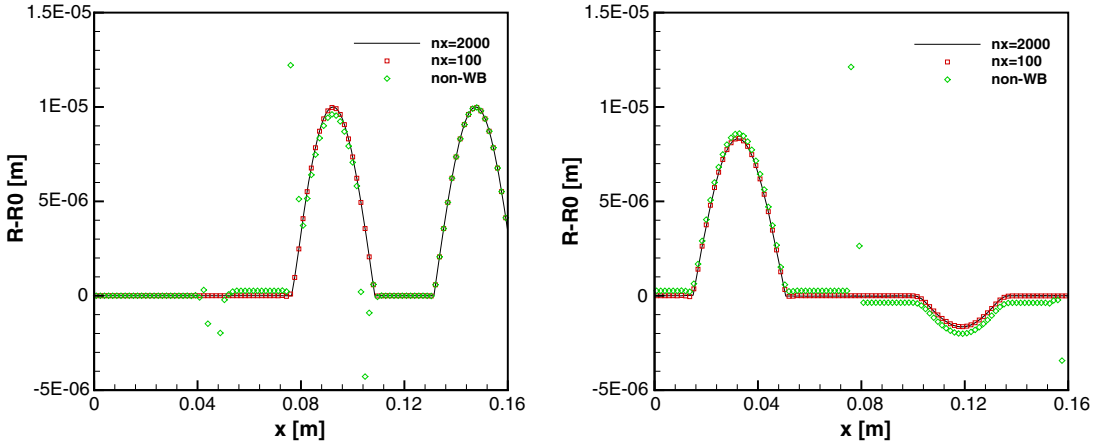

FIGURE 9 DG method: The numerical solutions of the propagation of a pulse to an expansion in Section 5.5 on a mesh with 100 cells and those of the non–well-balanced (denoted by non-WB) method. The errors $R - R_0$ at $t = 0.002$ seconds (left) and $t = 0.006$ seconds (right) [Colour figure can be viewed at wileyonlinelibrary.com]

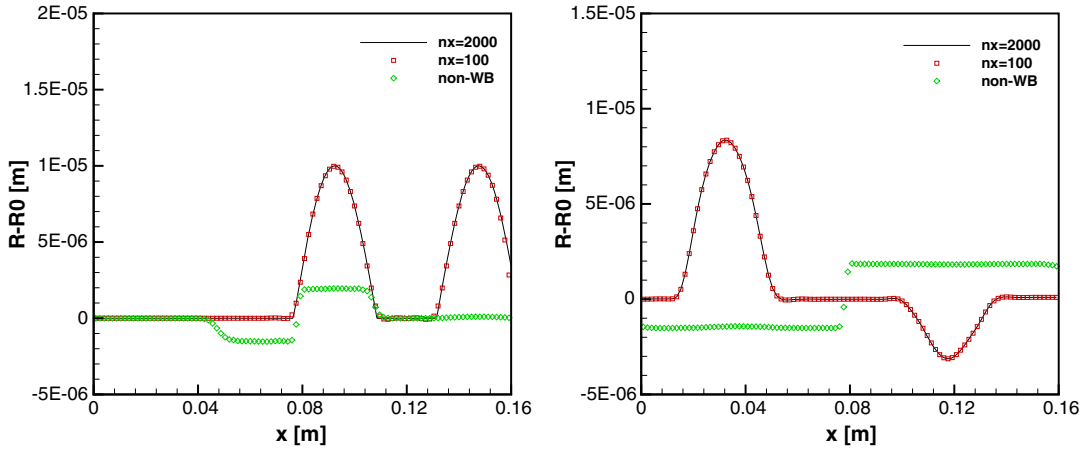

FIGURE 10 WENO scheme: The numerical solutions of the propagation of a pulse to an expansion in Section 5.5 on a mesh with 100 cells and those of the non–well-balanced (denoted by non-WB) scheme. The errors $R - R_0$ at $t = 0.002$ seconds (left) and $t = 0.006$ seconds (right) [Colour figure can be viewed at wileyonlinelibrary.com]

to the left and the other one going to the right at time $t = 0.002$ seconds. The numerical solutions of the well-balanced method are in good agreement with the reference ones and are comparable with those in Delestre and Lagrée.[12] However, the numerical results by the non–well-balanced ones fail to be good agreement with the reference solutions.

5.6 | Propagation of a pulse from an expansion

Then, we consider a pulse propagating from an expansion. The parameters are the same as in Section 5.5, only the initial radius is changed:

$$R(x,0) = \begin{cases} R_0(x)\left[1 + \epsilon \sin\left(\frac{100}{20L}\pi\left(x - \frac{15L}{100}\right)\right)\right] & \text{if } x \in \left[\frac{15L}{100}, \frac{35L}{100}\right], \\ R_0(x) & \text{else,} \end{cases}$$

with $\epsilon = 5.0 \times 10^{-3}$. Similarly, we also impose this problem with transmissive boundary conditions.

We present the initial error $R - R_0$ at time $t = 0$ seconds in Figure 11 and demonstrate the numerical results against the reference solutions at $t = 0.002$ seconds and $t = 0.006$ seconds, respectively, in Figures 12 and 13. Similarly, the numerical solutions of the well-balanced method fit well with the reference ones and are comparable with those in Delestre and Lagrée.[12] For comparison, we also plot the numerical results by the non–well-balanced ones. Nevertheless, the numerical results by the non–well-balanced ones do not fit well with the reference solutions.

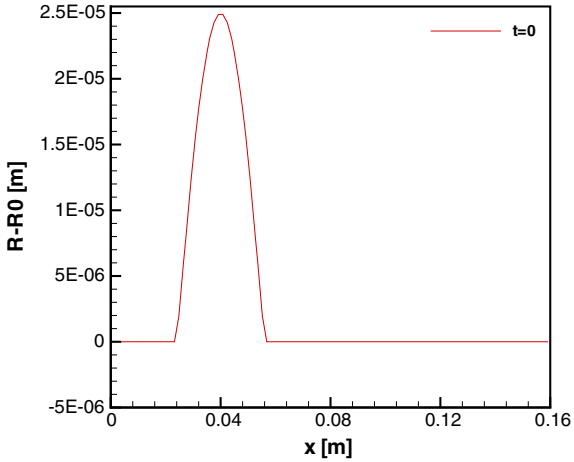

FIGURE 11 The initial error $R - R_0$ of the propagation of a pulse from an expansion in Section 5.6 [Colour figure can be viewed at wileyonlinelibrary.com]

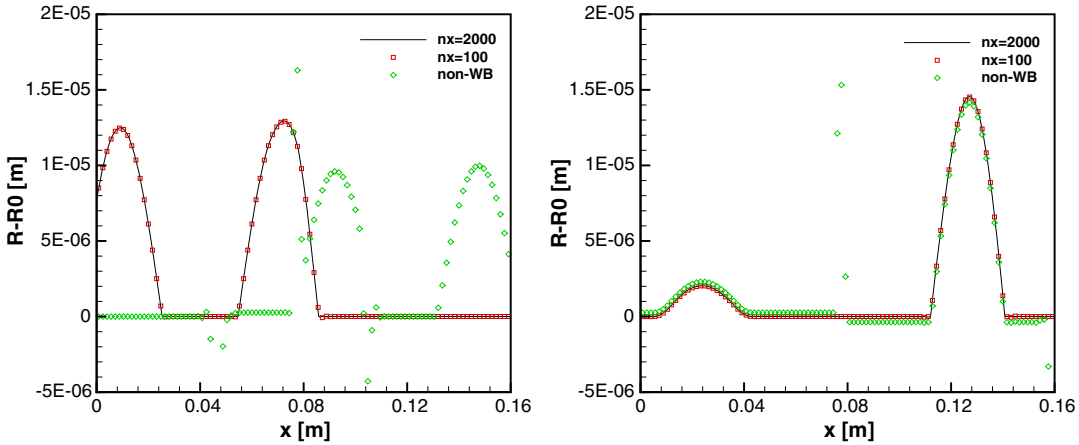

FIGURE 12 DG method: The numerical solutions of the propagation of a pulse from an expansion in Section 5.6 on a mesh with 100 cells and those of the non–well-balanced (denoted by non-WB) method. The errors $R - R_0$ at $t = 0.002$ seconds (left) and $t = 0.006$ seconds (right) [Colour figure can be viewed at wileyonlinelibrary.com]

5.7 | Wave damping

In this last test case, we look at the viscous damping term in the linearized momentum equation, which is an analogue of the Womersley problem.[40] We consider the following model coupled with the linear friction term:

$$\begin{cases} A_t + Q_x = 0, \\ Q_t + \left(\frac{Q^2}{A} + \frac{K}{3\rho\sqrt{\pi}}A^{\frac{3}{2}}\right)_x = \frac{KA}{2\rho\sqrt{\pi}\sqrt{A_0}}(A_0)_x - C_f\frac{Q}{A}, \end{cases} \tag{27}$$

where $C_f = 8\pi\nu$ with ν being the blood viscosity. We consider this example on a computational domain $[0, 3]$ subject to the given initial conditions

$$\begin{cases} A(x, 0) = \pi R_0^2, \\ Q(x, 0) = 0, \end{cases}$$

companied by the following parameters: $K = 1 \times 10^8$ Pa/m, $\rho = 1060$ kg/m^3, $R_0 = 4 \times 10^{-3}$ m. For the friction term, we directly apply the high order Gaussian quadrature rule.[32]

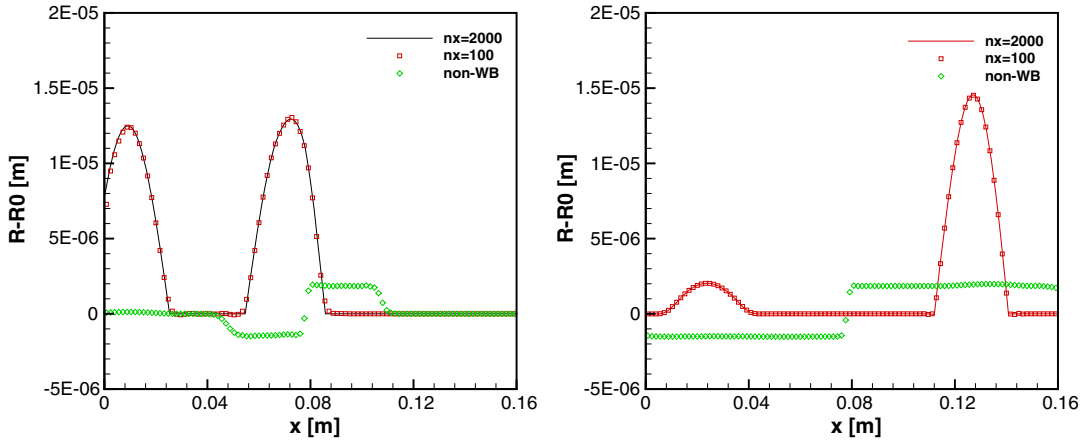

FIGURE 13 WENO scheme: The numerical solutions of the propagation of a pulse from an expansion in Section 5.6 on a mesh with 100 cells and those of the non–well-balanced (denoted by non-WB) scheme. The errors $R - R_0$ at $t = 0.002$ seconds (left) and $t = 0.006$ seconds (right) [Colour figure can be viewed at wileyonlinelibrary.com]

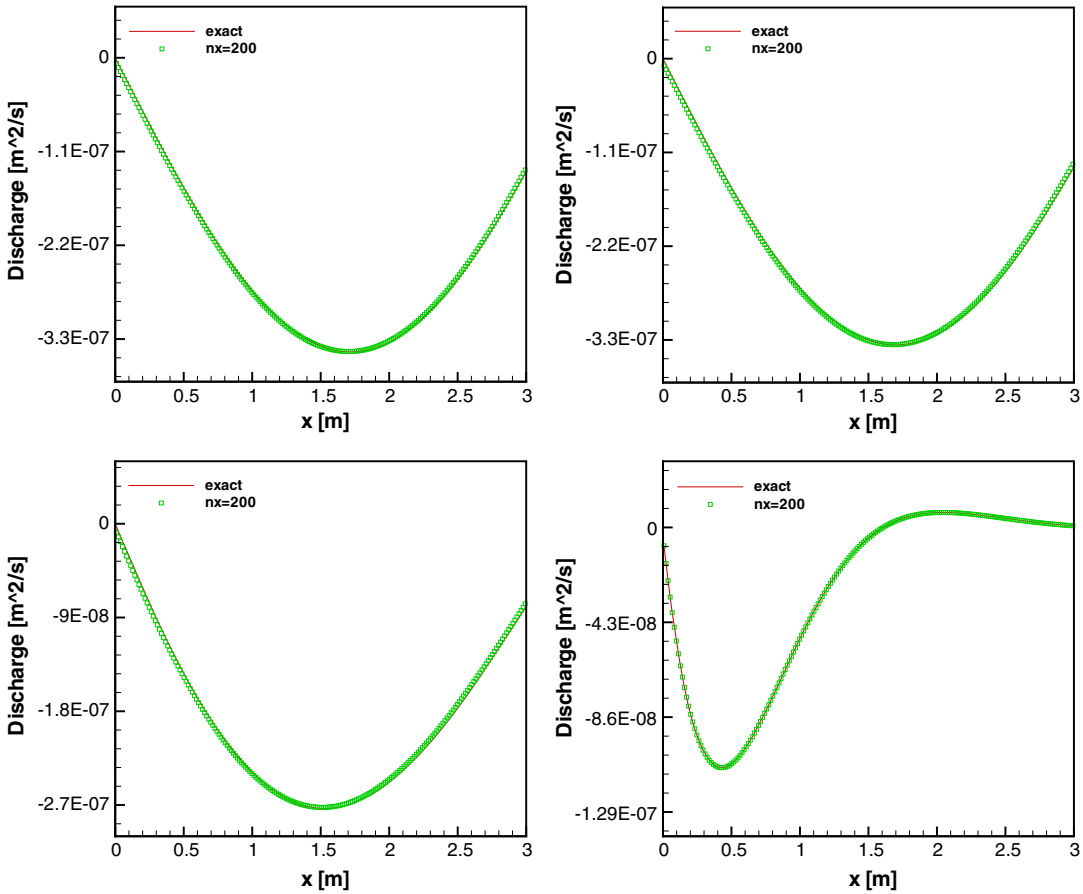

FIGURE 14 DG method: The numerical solutions of the wave damping in Section 5.7 on a mesh with 200 cells at $t = 25$ seconds. The damping of a discharge wave with $C_f = 0$ (upper left), $C_f = 0.000022$ (upper right), $C_f = 0.000202$ (lower left), and $C_f = 0.005053$ (lower right) [Colour figure can be viewed at wileyonlinelibrary.com]

Subsequently, we obtain a damping wave in the computational domain[12]

$$Q(t,x) = \begin{cases} 0 & \text{if } k_r x > \omega t, \\ Q_{\text{amp}} \sin(\omega t - k_r x) e^{k_i x} & \text{if } k_r x \le \omega t, \end{cases} \tag{28}$$

with

$$lclk_r = \left[\frac{\omega^4}{c_0^4} + \left(\frac{\omega C_f}{\pi R_0^2 c_0^2}\right)^2\right]^{\frac{1}{4}} \cos\left(\frac{1}{2}\arctan\left(-\frac{C_f}{\pi R_0^2 \omega}\right)\right),$$

$$k_i = \left[\frac{\omega^4}{c_0^4} + \left(\frac{\omega C_f}{\pi R_0^2 c_0^2}\right)^2\right]^{\frac{1}{4}} \sin\left(\frac{1}{2}\arctan\left(-\frac{C_f}{\pi R_0^2 \omega}\right)\right),$$

$$w = 2\pi/T_{\text{pulse}} = 2\pi/0.5\ s,$$

$$c_0 = \sqrt{\frac{k\sqrt{A_0}}{2\rho\sqrt{\pi}}} = \sqrt{\frac{kR_0}{2\rho}}.$$

For the treatment of the boundary conditions, we impose the incoming discharge

$$Q_b(t) = Q_{\text{amp}} \sin(wt)\ m^3/s,$$

at $x = 0$ m with $Q_{\text{amp}} = 3.45 \times 10^{-7}$ m^3/s being the amplitude of the inflow discharge.

In Figures 14 and 15, we present the numerical results against the exact solutions at $t = 25$ seconds with different C_f. It is obvious that the numerical solutions of the well-balanced method are in good agreement with the exact solutions and are comparable with those in Delestre and Lagrée.[12]

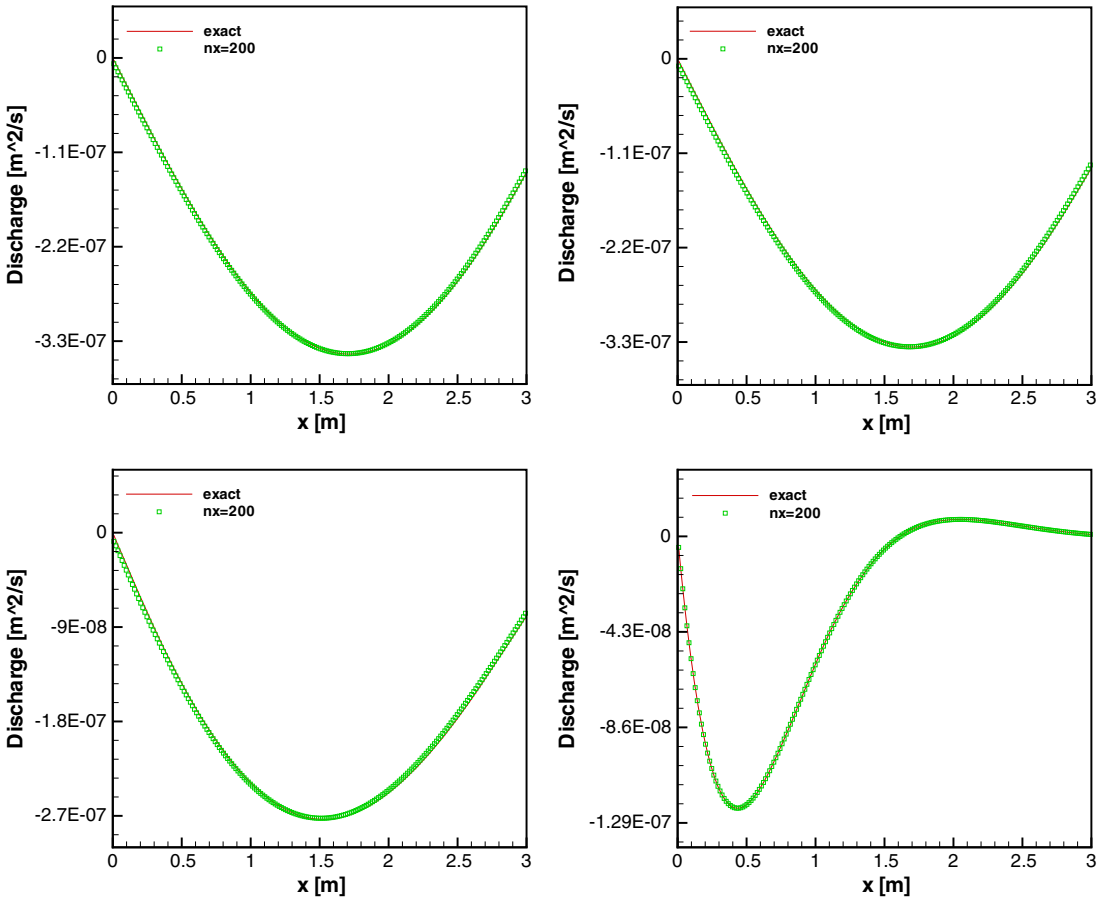

FIGURE 15 WENO scheme: The numerical solutions of the wave damping in Section 5.7 on a mesh with 200 cells at $t = 25$ seconds. The damping of a discharge wave with $C_f = 0$ (upper left), $C_f = 0.000022$ (upper right), $C_f = 0.000202$ (lower left), and $C_f = 0.005053$ (lower right) [Colour figure can be viewed at wileyonlinelibrary.com]

6 | CONCLUDING REMARKS

In this paper, we present a new class of high order well-balanced DG method and finite volume WENO scheme based on hydrostatic reconstruction for the blood flow model. Rigorous theoretical analysis as well as extensive numerical examples all suggest that the current DG method and finite volume WENO scheme maintain the well-balanced property, enjoy the high order of accuracy, and keep non-oscillatory shock resolution at the same time.

ACKNOWLEDGEMENTS

The research of the first author is supported by the Natural Science Foundation of PR China (11201254, 11401332 and 11771228) and the Project for Scientific Plan of Higher Education in Shandong Province of PR China (J12LI08). The research of the third author is supported by the state key program for developing basic sciences of PR China (2010CB731505) and Natural Science Foundation of PR China (11321061 and 11261160486). The authors would like to thank A. Ghigo for fruitful discussion.

ORCID

Gang Li http://orcid.org/0000-0002-0616-6859

REFERENCES

1. Formaggia L, Lamponi D, Tuveri M, Veneziani A. Numerical modeling of 1D arterial networks coupled with a lumped parameters description of the heart. *Comput Meth Biomech Biomed Eng*. 2006;9:273-288.
2. Kolachalama VB, Bressloff NW, Nair PB, Shearman CP. Predictive haemodynamics in a one-dimensional human carotid artery bifurcation. Part I: application to stent design. *IEEE Trans Biomed Eng*. 2007;54:802-812.
3. Lagrée PY. An inverse technique to deduce the elasticity of a large artery. *Eur Phys J*. 2000;9:153-163.
4. Lagrée PY, Lorthois S. The RNS/PRANDTl equations and their link with other asymptotic descriptions. Application to the computation of the maximum value of the wall shear stress in a pipe. *Int J Eng Sci*. 2005;43:352-378.
5. Bouchut F. *Nonlinear stability of finite volume methods for hyperbolic conservation laws, and well-balanced schemes for sources*. Birkhäuser: Frontiers in Mathematics series; 2004.
6. Xiu D, Sherwin SJ. Parametric uncertainty analysis of pulse wave propagation in a model of a human arterial network. *J Comput Phys*. 2007;226:1385-1407.
7. Greenberg JM, LeRoux AY. A well-balanced scheme for the numerical processing of source terms in hyperbolic equations. *SIAM J Numer Anal*. 1996;33:1-16.
8. Xing YL, Shu CW, Noelle S. On the advantage of well-balanced schemes for moving-water equilibria of the shallow water equations. *J Sci Comput*. 2011;48:339-349.
9. Noelle S, Xing YL, Shu C-W. High-order well-balanced schemes. In: Puppo G, Russo G, eds. *Numerical Methods for Balance Laws*. Italy: Dipartimento di Matematica, Seconda Universita di Napoli; 2010:1-64.
10. Sherwin SJ, Formaggia L, Peiró J, Franke V. Computational modelling of 1D blood flow with variable mechanical properties and its application to the simulation of wave propagation in the human arterial system. *Int J Numer Methods Fluids*. 2003;43:673-700.
11. Wang X, Fullana JM, Lagrée PY. Verification and comparison of four numerical schemes for a 1D viscoelastic blood flow model. *Comput Meth Biomech Biomed Eng*. 2015;18:1704-1725.
12. Delestre O, Lagrée PY. A 'well-balanced' finite volume scheme for blood flow simulation. *Int J Numer Methods Fluids*. 2013;72:177-205.
13. Wibmer M. One-dimensional simulation of arterial blood flow with applications. *PhD Thesis*: eingereicht an der Technischen Universitat Wien, Fakultat fur Technische Naturwissenschaften und Informatik; January 2004.
14. Caleffi N, Cavallini. V, Coscia V. Finite volume and WENO scheme in one-dimensional vascular system modelling. *Comput Math Appl*. 2008;56:2382-2397.
15. Cavallini N, Coscia C. One-dimensional modelling of venous pathologies: finite volume and WENO schemes. In: Rannacher R, Sequeira A, eds. *Advances in Mathematical Fluid Mechanics*. Berlin Heidelberg: Springer; 2010:147-170..
16. Müller LO, Parés C, Toro EF. Well-balanced high-order numerical schemes for one-dimensional blood flow in vessels with varying mechanical properties. *J Comput Phys*. 2013;242:53-85.
17. Murillo J, García-Navarro P. A Roe type energy balanced solver for 1D arterial blood flow and transport. *Comput Fluids*. 2015;117:149-167.
18. Wang ZZ, Li G, Delestre O. Well-balanced finite difference weighted essentially non-oscillatory schemes for the blood flow model. *Int J Numer Methods Fluids*. 2016;82:607-622.
19. Audusse E, Bouchut F, Bristeau MO, Klein R, Perthame B. A fast and stable well-balanced scheme with hydrostatic reconstruction for shallow water flows. *SIAM J Sci Comput*. 2005;25:2050-2065.

20. Noelle S, Pankratz N, Puppo G, Natvig JR. Well-balanced finite volume schemes of arbitrary order of accuracy for shallow water flows. *J Comput Phys*. 2006;213:474-499.
21. Xing YL, Shu CW. A new approach of high order well-balanced finite volume WENO schemes and discontinuous Galerkin methods for a class of hyperbolic systems with source terms. *Commun Comput Phys*. 2006;1:100-134.
22. LeVeque RJ. Balancing source terms and flux gradients on high-resolution Godunov methods: the quasi-steady wave-propagation algorithm. *J Comput Phys*. 1998;146:346-3658.
23. Perthame B, Simeoni C. A kinetic scheme for the Saint-Venant system with a source term. *Calcolo*. 2001;38:201-231.
24. Xu K. A well-balanced gas-kinetic scheme for the shallow-water equations with source terms. *J Comput Phys*. 2002;178:533-562.
25. Xing YL, Shu CW. High order finite difference WENO schemes with the exact conservation property for the shallow water equations. *J Comput Phys*. 2005;208:206-227.
26. Xing YL, Shu CW. A survey of high order schemes for the shallow water equations. *J Math Study*. 2014;47:221-2494.
27. Tian CT, Xu K, Chan KL, Deng LC. A three-dimensional multidimensional gas-kinetic scheme for the Navier-Stokes equations under gravitational fields. *J Comput Phys*. 2007;226:2003-2027.
28. Xu K, Luo J, Chen S. Well-balanced kinetic scheme for gas dynamic equations under gravitational field. *Adv Appl Math Mech*. 2010;2:200-210.
29. Luo J, Xu K, Liu N. A well-balanced symplecticity-preserving gas-kinetic scheme for hydrodynamic equations under gravitational field. *SIAM J Sci Comput*. 2011;33:2356-2381.
30. Xing YL, Shu CW. High order well-balanced WENO scheme for the gas dynamics equations under gravitational fields. *J Sci Comput*. 2013;54:645-662.
31. Käppeli R, Mishra S. Well-balanced schemes for the Euler equations with gravitation. *J Comput Phys*. 2014;259:199-219.
32. Cockburn B, Karniadakis G, Shu CW. The development of discontinuous Galerkin methods. In: Cockburn B, Karniadakis G, Shu CW, eds. *Discon- tinuous Galerkin Methods: Theory, Computation and Applications, Lecture Notes in Computational Science and Engineering, Part I: Overview*. Berlin Heidelberg: Springer; 2000:3-50.
33. Cockburn B, Shu CW. Runge-Kutta discontinuous Galerkin methods for convection dominated problems. *J Sci Comput*. 2001;16:173-261.
34. Shu CW. Essentially non-oscillatory and weighted essentially non-oscillatory schemes for hyperbolic conservation laws. *Advanced Numerical Approximation of Nonlinear Hyperbolic Equations*, Lecture Notes in Mathematics, Vol. 1697. Berlin Heidelberg: Springer; 1998:325-432.
35. Shu CW. High order weighted essentially non-oscillatory schemes for convection dominated problems. *SIAM Review*. 2009;51:82-126.
36. Shu CW. High order WENO and DG methods for time-dependent convection-dominated PDEs: A brief survey of several recent developments. *J Comput Phys*. 2016;316:598-613.
37. Shu CW, Osher S. Efficient implementation of essentially non-oscillatory shock-capturing schemes. *J Comput Phys*. 1988;77:439-471.
38. Xing YL, Shu CW. High order well-balanced finite volume WENO schemes and discontinuous Galerkin methods for a class of hyperbolic systems with source terms. *J Comput Phys*. 2006;214:567C598.
39. Delestre O, Lucas C, Ksinant PA, et al. SWASHES: a compilation of shallow water analytic solutions for hydraulic and environmental studies. *Int J Numer Methods Fluids*. 2013;72:269-300.
40. Womersley J. On the oscillatory motion of a viscous liquid in thin-walled elastic tube: I. *Philos Mag*. 1955;46:199-221.

How to cite this article: Li G, Delestre O, Yuan L. Well-balanced discontinuous Galerkin method and finite volume WENO scheme based on hydrostatic reconstruction for blood flow model in arteries. *Int J Numer Meth Fluids*. 2017;1–18. https://doi.org/10.1002/fld.4463